Journal of Thermal Analysis and Calorimetry, Vol. 95 (2009) 2, 445–454

THERMAL DEGRADATION OF IRON CHELATE COMPLEXES ADSORBED ON MESOPOROUS SILICA AND ALUMINA

Z. Gabelica[1], A. Charmot[2], R. Vataj[1], R. Soulimane[3], J. Barrault[2] and S. Valange[2]*

[1]LPI-GSEC, ENSCMu, 3 Rue A. Werner, 68093 Mulhouse Cedex, France
[2]Université de Poitiers, ESIP, CNRS-LACCO, UMR 6503, 40 Av. Recteur Pineau, 86022 Poitiers, France
[3]Laboratoire de Catalyse et Synthèse en Chimie Organique (LCSCO), B.P. 119, Université A. Belkaid, Tlemcen 13000, Algérie

Nanometric Fe_2O_3 particles could be inserted inside the internal pore volume of SBA-15 mesoporous silica and mesoporous alumina supports, when Fe(III) chelates (EDTA, gluconate or citrate) were used as impregnating precursors. The oxidative degradation of the chelating anions was followed by combined TG-DTA. Strong chelate-SiOH interactions (case of bulky EDTA), favored by the mesopore curvature, yield sub-nanometric extremely well dispersed Fe_2O_3 particles preferentially located at the micropore mouths (confinement effect). Fe_2O_3 even more strongly interacts with alumina walls, generating either $(Fe,Al)_2O_3$ mixed phases or Fe-aluminate micro domains. These iron-based mesoporous alumina composites proved very active catalysts in total oxidation of phenol at ambient conditions, with extremely low iron leaching (0.2%).

Keywords: *confinement effect, Fe_2O_3 nanoparticles, Fe_2O_3/SBA-15 composites, iron chelate thermal degradation, mesoporous alumina*

Introduction

Iron-based catalysts proved very efficient for many catalytic reactions, such as nitrogen oxide removal, several acid-assisted transformations of organic substrates (e.g., Friedel–Crafts reactions, isomerizations, …) or for various oxidations [1–5].

Their overall performance is strongly dependent on the dispersion of the active phase (e.g. Fe_2O_3) onto the support (silica, alumina, …), a property that is quite difficult to control in the case of iron. Organized mesoporous solids, into which the active phase can be inserted (dispersed), represent attractive supports, combining interesting textural properties and a high surface area.

Different routes are currently used to introduce Fe_2O_3 active sites on a substrate, for example by ion exchange [6], impregnation, co-precipitation [7], grafting [8], direct hydrothermal synthesis [9], sol–gel technique [10, 11], equilibrium-adsorption method [12], thermal decomposition of metal-organic precursors [13] or by using less conventional technologies such as CVD [14], plasma-spray, PVD, laser pyrolysis [15] and supercritical preparations [16]. The real difficulty consists in obtaining a uniform dispersion of the active centers over the support surface, as well as the decrease of the Fe_2O_3 particles size down to the nanometric range. This could result in properties (magnetic behavior, thermal stability, reactivity, catalytic applications, …) that are not achieved with the corresponding bulk oxides.

Several groups have also tried to pattern iron oxide particles in different periodic mesoporous silicas, such as wormhole (HMS [17]), hexagonal (MCM-41 [18, 19], SBA-15 [20–22]) and cubic (MCM-48, KIT-5, KIT-6 [21, 23]) mesostructures. The pores of these silicas are well-calibrated, with mesopore diameters which can be adjusted between 4 and 10 nm. While organized mesoporous solids could be advantageously used as substrates to increase the dispersion of the active centers (metallic or oxidic nanoparticles) compared to bulk supports, it has been established that the location, dispersion, reductive properties, as well as the state of iron oxide nanoparticles are affected by the pore topology of the (mesoporous) carrier, and by the preparation method used [21]. The presence of well-developed pore structures of the host matrix seems to be of primary importance for the stabilization of iron oxide nanoparticles inside the mesopores. However, exclusive location of the metal oxide particles within the pores of the host matrix, coupled to a high level of nanoparticle dispersion, was shown to be difficult to control for some of the samples prepared by wet impregnation using classical iron precursors [21].

In this respect, an interesting procedure leading to the simultaneous control of the size and dispersion of oxidic nanoparticles consists in impregnating various (bulky) supports with metal chelating precursors, as

* Author for correspondence: sabine.valange@univ-poitiers.fr

1388–6150/$20.00

Akadémiai Kiadó, Budapest, Hungary
Springer, Dordrecht, The Netherlands

suggested by Meima *et al.* [24]. Furthermore, Lensveld *et al.* [25] succeeded in dispersing very small nickel oxide particles on the MCM-41 mesoporous silica surface, by using an aqueous solution of nickel citrate. These authors have shown that the insertion of aqueous solutions of multidentate chelated metal complexes into the ordered pore structure of various mesophases, followed by a controlled calcination step, resulted in uniform distributions of highly dispersed metal oxidic residues over the support. According to van Dillen *et al.* [26], the driving force for the final dispersion of the oxide nanoparticles upon evaporation of the impregnated metal chelate solution, could be the formation of a gel-like phase that favors a preliminary dispersion of the chelate over the substrate surface as a film, after full drying, thereby preventing a further sintering of the resulting oxidic particles after thermal degradation of the metal chelate. No mechanism describing the successive interactions of either the precursor (metal chelate) or of the final metal oxide particles with the support was proposed.

In the scope of an extended research in environmental catalysis conducted in our laboratories and concerning the use of iron-containing materials with controlled open structures, we have recently reported the preparation and characterization of a series of SBA-15 mesoporous silica-supported iron oxide composite catalysts, using the chelate route [27]. Three different bulky iron chelates, namely (Fe(III),Na)-EDTA, (Fe(III),NH_4)-citrate and Fe(II)-gluconate, were inserted into the silica internal pore volume using the classical incipient wetness impregnation method, and compared with a non-chelating iron salt, namely Fe(III) nitrate. This procedure was shown to lead to a uniform dispersion of Fe_2O_3 (sub)nanometric particles inside the porosity of SBA-15 silica, hereafter referred to as Fe_2O_3/SBA-15 composites.

Here we wish to investigate more in depth the actual mechanism through which such iron chelate precursors interact with the surface silanol groups of the mesoporous silica, as a function of temperature. Combined TG-DTA was first used to follow in a controlled way the thermal degradation of the chelate anions and to define the (temperature) conditions under which the residual quasi atomically dispersed Fe(III) oxidic particles start to form and to interact with the substrate surface. XRD, TEM/EDX, electron micro-diffraction, sorption isotherms and TPR were used to complementary characterize the final size, dispersion and location of the so generated Fe_2O_3 particles, assuming that the micropores running perpendicularly to the substrate mesoporous walls could act as traps to selectively quench and stabilize them through a confinement-type effect [28].

The iron-chelate route was further extended in the case of mesoporous alumina that, because of its more pronounced basic character than silica, is expected to even more strongly interact with Fe(III) oxides that rather behave as intrinsic acid centers.

Catalytic performances of all the composites were evaluated in the case of total phenol oxidation by H_2O_2 in aqueous solution (heterogeneous Fenton reaction).

Experimental

Composite preparation

Pure siliceous mesoporous SBA-15 was prepared using a literature procedure [29]. The surfactant, Pluronic P123, was dissolved in a mixture of water and HCl at 40°C. Tetraethylorthosilicate (TEOS) was added to the surfactant solution and the mixture stirred for 24 h. It was then transferred to Teflon bottles and heated at 100°C for 3 days. The white solid was filtered, washed with distilled water, air-dried and calcined at 550°C for 8 h under flowing air.

Mesoporous alumina materials were synthesized in aqueous solution at room temperature following a home-elaborated original recipe [30], in the presence of Keggin-type aluminum polycations and neutral surfactants belonging to the alkylamine-N-oxide family. The solids were recovered by filtration, washed with a small amount of water, dried at 60°C and air-calcined at 500°C for 6 h.

Dispersed Fe_2O_3/substrate composites were generated through a TG/DTA-controlled calcination of SBA-15 or mesoporous alumina supports containing different Fe(II) and Fe(III) chelate precursors, namely (Fe(III),Na)-EDTA, (Fe(III),NH_4)-citrate and Fe(II)-gluconate, as well as Fe(III) nitrate, used for comparison. Before being used as support, the calcined mesoporous material (silica and alumina) was preliminary dehydrated into a Schlenck reactor under vacuum at 120°C during 4 h. The chelate precursors were then inserted at room temperature into the silica or alumina support through incipient wetness impregnation. This technique is based on the addition of a volume of aqueous solution containing the iron precursor equal to the porous volume of the support determined by nitrogen sorption. An aqueous $Fe(NO_3)_3 \cdot 9H_2O$ or Fe(III) chelate solution of variable concentration was used to prepare the Fe-loaded silica and alumina samples. The solution concentration was adjusted in each impregnation step so as to correspond to a complete filling of the substrate pore volume and achieve, after two successive impregnations, the final atomic Fe/Si or Fe/Al ratios to 0.05, corresponding to 5 mass% Fe. The impregnated solids were dried in air for 2 h at

80°C, then for 12 h at 120°C, before being activated up to 450°C under air flow (10 L h^{-1} g^{-1}) so as to completely decompose the chelate (or nitrate) anions, and generate the corresponding supported Fe(III) oxidic phases.

Characterization

Powder XRD patterns of the calcined Fe_2O_3/SBA-15 and Fe/mesoporous Al_2O_3 composites were recorded on a Bruker D5005 diffractometer with monochromatized CuK_α radiation (λ=1.5418 Å) at 40 kV, 30 mA. Bulk chemical analysis for Fe, Si and Al was achieved by ICP. TG-DTA study of the decomposition sequence in flowing air of the pure and supported chelates was performed on a SDT 2926 microbalance from 20 to 700°C at a heating rate of 5°C min^{-1}. The surface area and pore size analysis of the composites was carried out by adsorption–desorption of nitrogen on a Micromeritics ASAP 2010 instrument (–196°C). Prior to N_2 adsorption, the samples were degassed under vacuum at 90°C for 1 h, followed by a further heating at 300°C for a few hours. The size of the iron oxide particles dispersed over the surface of Fe_2O_3/SBA-15 and of Fe_2O_3/mesoporous Al_2O_3 composites, was evaluated by TEM (Philips CM120 microscope) coupled to an EDX analyzer (fixed probe) for Fe spot detection over the sample surface. Electron microdiffraction patterns were also recorded to identify the structure of the iron-bearing particles. The samples were at first included in a resin that was cut into sections of 30 to 50 nm with a microtome equipped with a diamond cutter, before dispersion on a carbon-coated gold grid. H_2-TPR measurements were performed on the calcined Fe/SBA-15 materials pre-treated in argon at 450°C for 1 h prior to heating under H_2 flow (5 vol% in Ar) from 20 to 900°C at a heating rate of 10°C min^{-1}. H_2 consumption was continuously monitored by a thermal conductivity detector.

Catalytic tests were performed in ambient conditions (at atmospheric pressure and at 25 or 40°C) in a thermostated semi-batch reactor of 250 mL using phenol as reactant and hydrogen peroxide as oxidant. The reactor was equipped with a pH electrode to continuously monitor the pH value of the reaction solution, close to its optimum value (pH≈3.7) as previously demonstrated [31]. The catalyst (100 mg) was put into 100 mL of an aqueous phenol solution ($5\cdot10^{-4}$ mol L^{-1}) under continuous strirring, 15 min before the beginning of the hydrogen peroxide addition. H_2O_2 solution (0.1 mol L^{-1}) was added continuously to the phenol solution at a constant flow rate of 2 mL h^{-1} through a dosimeter (Dosimat 725 Metrohm). The reaction was performed under air flow (2 L h^{-1}) bubbling directly through the reaction solution in order to maintain the amount of dissolved oxygen close to its saturation concentration. Phenol conversion as well as the products formed by the reaction were determined during the overall reaction (4 h) using a high performance liquid chromatography (Waters HPLC) equipped with an Aminex HPX-87 (Biorad) column. The total organic carbon (TOC) content was measured by a DC-190 Dohrmann TOC meter [32].

Results and discussion

Structure and morphology of calcined Fe_2O_3/silica composites

X-ray diffractograms (spectra not shown) confirmed (low angle domain) that the hexagonal ordering in the SBA-15 silica was retained after the impregnation/calcination steps, in contrast with the thin walled MCM-41 that rapidly collapsed under such conditions [33]. At wide angles, the sample prepared using iron nitrate as Fe_2O_3 precursor displayed intense, well-resolved XRD lines, readily attributed to α-Fe_2O_3 and suggesting that relatively large particles are present. The presence of hematite was duly confirmed by electron microdiffraction.

In contrast, no discernable iron oxide reflections were visible on the diffractograms of the three calcined composites prepared using the chelate complexes, suggesting the exclusive presence of very small nanometric Fe(III) oxidic particles that cause the classical line broadening on the XRD patterns. The real presence of such particles was unambiguously confirmed by spot EDX probing (see below). The extremely small size of these particles prevented their further identification by electron diffraction, thereby not excluding the presence of either α-Fe_2O_3 (hematite) or γ-Fe_2O_3 (maghemite), or both. Maghemite has been already detected in similar systems [22].

TEM investigation of Fe_2O_3 particle location within the calcined SBA-15 composites revealed that in neither case Fe_2O_3 large clusters coated the external surface of silica (as in the case of wet impregnation [33]). The thermal decomposition of the nitrate precursor led to the rapid generation of α-Fe_2O_3 particles which migrate through the SBA-15 channels during the evaporation of the last solvent traces, resulting in agglomerates of which the size was limited by the silica pore diameter (8 nm). Each mesopore was shown to be plugged by one Fe_2O_3 particle on average (Fig. 1a).

In contrast, in the chelate cases, spot EDX analyses confirmed the presence of very small Fe particles (presumably belonging to Fe_2O_3-type species) homogeneously dispersed throughout the mesoporous silica matrix but hardly visible under TEM conditions (Fe(II)-gluconate [33], figure not shown here). Such

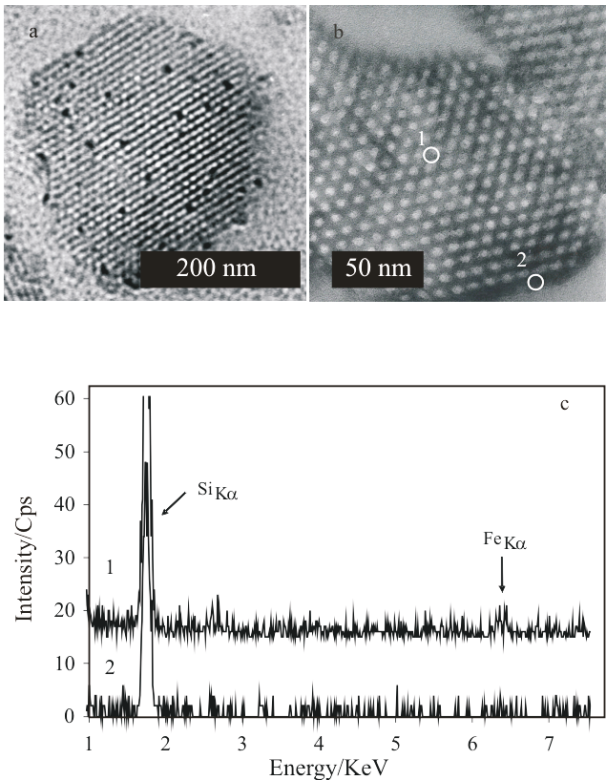

Fig. 1 TEM images of SBA-15-supported iron oxide catalysts prepared using a – Fe(III) nitrate, b – (Fe(III),Na)-EDTA chelate precursor and c – the corresponding EDX spot analyses of two selected areas of sample b), as numbered on the TEM image

particles were even smaller (<2.5 nm) for the sample prepared in the presence of (Fe(III),NH_4)-citrate, suggesting an increased chelating efficiency of the citrate anion, compared to that of the gluconate [27], as confirmed here by combined TG-DTA (see below).

This trend was even more pronounced when (Fe(III),Na)-EDTA was used as iron precursor. In this case indeed, while iron oxide particles could never be visualized by TEM, EDX analyses throughout the silica matrix still did confirm that iron species were present, presumably homogeneously dispersed inside the SBA-15 mesopores, thereby implying the presence of sub-nanometric, TEM-silent Fe_2O_3 particles (Figs 1b and c).

These results suggested that the size of Fe_2O_3 generated after subsequent oxidation of the chelates could be tuned from nanometric to sub-nanometric dimensions, depending on the nature (geometry) of the chelate complex used as precursor.

Thermal degradation of chelate anions (combined TG-DTA)

The decomposition sequences in oxidative atmosphere of the pure Fe(II)-gluconate, (Fe(III),NH_4)-citrate, (Fe(III),Na)-EDTA and of Fe(III) nitrate, used as 'blank' non-chelating compound, were first recorded (TG curves) so as to select the common temperature at which the Fe_2O_3 residues (with possible traces of $NaFeO_2$ in the case of Fe(III),Na-EDTA chelate) are stabilized. It appeared that, at 450°C, the degradation of all anions was complete and corresponded to the theoretical mass losses (Table 2, Fig. 2).

The same decomposition was then similarly monitored using combined TG-DTA for the 3 composites prepared through incipient wetness impregnation of pre-calcined SBA-15 substrate with the three iron chelates and with Fe(III) nitrate. The aim was to evaluate in each case the degree of interaction of the precursor with the silica surface that should be related

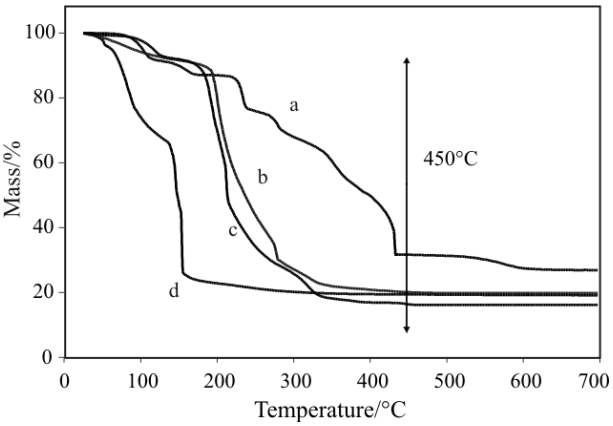

Fig. 2 TG trace of several pure iron chelates
a – (Fe(III),Na)-EDTA, b – (Fe(III),NH_4)-citrate, c – Fe(II)-gluconate and d – Fe(III) nitrate hexahydrate

Table 1 Textural properties of various calcined Fe_2O_3/SBA-15 composites

Precursor	S_{BET}/ $m^2\ g^{-1}$	Microporous volume/ $cm^3\ g^{-1}$	Mesoporous volume/ $cm^3\ g^{-1}$
SBA-15	810	0.077	1.11
Fe(III) nitrate/SBA-15	770	0.081	1.03
Fe(II)-gluconate/SBA-15	673	0.032	0.72
(Fe(III),NH_4)-citrate/SBA-15	620	0.046	0.80
(Fe(III),Na)-EDTA/SBA-15	486	0	0.64

Table 2 TG-DTA data related to the oxidative degradation of the pure chelating anions and their decomposition sequence in oxidative atmosphere

Chelate	Mass loss/%		Decomposition sequences
	Theor.	Exp.	
Fe(II)-gluconate	75.9	75.4	$Fe(C_6H_{11}O_7 \cdot H_2O)_2 \rightarrow FeO_{3/2}$ 1 DTA endotherm at 123°C (dehydration), 2 exotherms at 210 and 319°C
(Fe(III),NH_4)-citrate	71.4	72.1	$Fe(NH_4)_{0.9}(C_6H_5O_7)_{1.3} \rightarrow Fe(C_6H_{11}O)_2 \rightarrow FeO_{3/2}$ 3 DTA exotherms at 275, 321 and 433°C
(Fe(III),Na)-EDTA	70.0	68.7	$FeNa \cdot C_{10}H_{12}O_8N_2 \rightarrow FeNaO_2$ Complex degradation scheme: 2 endotherms at 108 and 165°C, then oxidative degradation starting at 220°C and ending at 432°C

Table 3 Decomposition temperature of various pure iron chelates and iron nitrate, of the same mechanically admixed with SBA-15 silica and of the same in interaction with the silica after impregnation

Sample	Effect	Temperature (°C)
Free Fe(III) nitrate hexahydrate	Dehydration	75
Fe(III) nitrate admixed with SBA-15		63
Fe(III) nitrate/SBA-15 composite		45
Free Fe(II)-gluconate	Anion decomposition	210
Fe(II)-gluconate admixed with SBA-15		207
Fe(II)-gluconate/SBA-15 composite		168
Free (Fe(III),NH_4)-citrate	Anion decomposition	275-321
(Fe(III),NH_4)-citrate admixed with SBA-15		274
(Fe(III),NH_4)-citrate/SBA-15 composite		200
Free (Fe(III),Na)-EDTA	Anion decomposition	432
(Fe(III),Na)-EDTA admixed with SBA-15		413
(Fe(III),Na)-EDTA /SBA-15 composite		223

to the temperature characterizing the DTA peaks corresponding to the anion degradation.

It was observed that the impregnated chelates systematically undergo decomposition at a lower temperature than their bulky (non supported) analogues (Table 3), suggesting their very efficient dispersion on the substrate (internal) surface during the early stages of the impregnation/drying processes and, subsequently, their probable optimized interaction with the substrate surface.

As a first example, Fig. 3 compares the TG-DTA patterns of pure Fe(III) nitrate and of Fe(III) nitrate impregnated on mesoporous SBA-15 silica. It is clearly seen from both TG traces and DTA endotherms (non oxidative degradation of nitrate ions at low temperature), that the free Fe(III) nitrate is decomposed at a higher temperature than when it is occluded in the silica mesopores.

The second example even more clearly confirms that effect for the (Fe(III),Na)-EDTA chelate (Fig. 4). Indeed, the main DTA exotherm (oxidative degradation of the EDTA macro anion at high temperature)

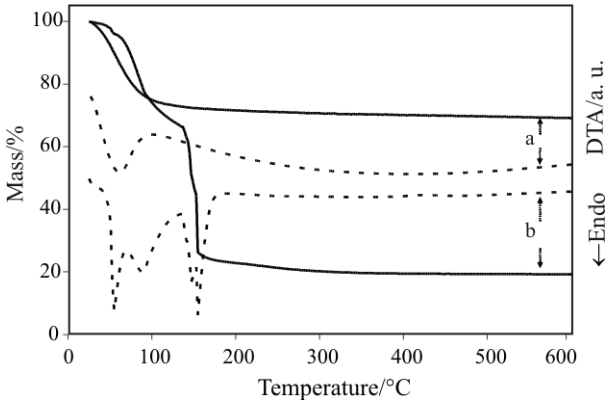

Fig. 3 — – TG - - - – DTA traces of a – Fe(III) nitrate in interaction with mesoporous SBA-15 silica after impregnationand b – free Fe(III) nitrate

also varies in the order: (Fe(III),Na)-EDTA/SBA-15 composite (223°C)<(Fe(III),Na)-EDTA mechanically admixed with SBA-15 (413°C)<bulk (Fe(III),Na)-EDTA (432°C), thus suggesting, as for the nitrate, that the stronger the interaction of the precursor with

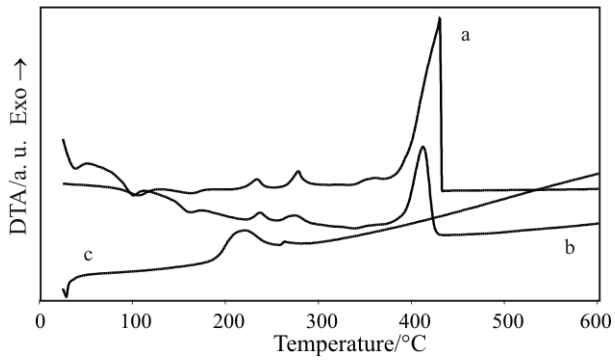

Fig. 4 DTA traces of a – free (Fe(III),Na)-EDTA, b – (Fe(III),Na)-EDTA mechanically admixed with SBA-15 silica and c – (Fe(III),Na)-EDTA in interaction with SBA-15 silica after impregnation

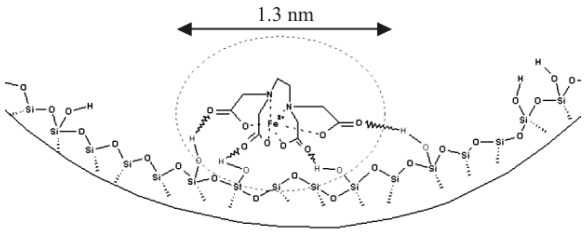

Fig. 5 Schematic view (on scale) of one molecule of (Fe(III),Na)-EDTA interacting with the superficial silanols present in SBA-15 silica mesopores

the silica surface, the easier its decomposition and thus the more prompt release of the Fe(III) oxidic residue.

This a priori surprising effect could be rationalized by considering that the highly dispersed chelate (and, to a lesser extent, nitrate), by lying flat onto the mesopore surface, would more promptly undergo hydrogen-type interactions with the superficial silanols. Such a stabilization of the organic anion (chelate case) inside the mesopores would first weaken its coordinative bonds with the Fe(III) cations that will readily transform into dispersed Fe_2O_3 nanoparticles on the surface. Through that kind of concerted effect, the anions, freed from their counterion, would then rapidly degrade at a relatively low temperature. The bulkier the anion, the better its initial pore coverage and thereby its consequent interaction with the surface silanols, the more rapidly it would decompose. Figure 5 schematically describes this concerted decomposition mechanism.

This concerted interaction of the chelate anions with Fe(III) cations (through coordinative bonds) and with the silica surface (through hydrogen bonds), explains the easier oxidative degradation of the chelate anions as soon as their bonds with Fe(III) counterions are weakened. Assuming that the ease of EDTA decomposition can be qualitatively evaluated by the temperature characterizing the corresponding DTA exotherms, one can measure that temperature difference (ΔT) between the free iron chelate and the same inserted in the corresponding iron chelate/SBA-15 composite (Table 3). The bulkier the anion (EDTA case), the larger the ΔT. From the less bulky gluconate to the most voluminous EDTA, the ΔT values indeed varied in the following sequence: 42°C (gluconate)<75°C (citrate)<209°C (EDTA) (curves from [33], not shown).

Stabilization of Fe_2O_3 nanoparticles by confinement effects

A systematic restriction of the S_{BET} surface area and of the mesoporous and microporous volumes was systematically observed in all iron chelate-impregnated substrates, especially for the sample impregnated with (Fe(III),Na)-EDTA (Table 1).

The regular decrease of the mesoporous volume firstly confirmed that Fe_2O_3 particles generated after subsequent oxidation of the various chelates were located inside the channels on both sides of the mesopore walls.

The fact that the mesopores of the composites prepared using the chelate route were hardly affected by the insertion of the Fe_2O_3 nanoparticles, suggests that the freshly generated oxidic species could have been preferentially deposited inside the silica micropores. Indeed, such micropores are abundant in SBA-15 specifically prepared using the described recipe [29, 34], which is substantiated by the significant values of the microporous volumes measured in the case of pure SBA-15 and for the Fe(III) nitrate/SBA-15 composite (Table 1).

It could be reasonably assumed that the freshly generated very small Fe oxidic species would preferentially deposit next to the silica micropore mouths or even inside the micropores, thus on positions where such sites exhibit a high curvature. A decrease of the micropore content of about 30% was observed for the sample prepared with Fe(II)-gluconate, while they totally disappeared for the sample synthesized in the presence of (Fe(III),Na)-EDTA, suggesting that, in this last case, Fe_2O_3 particles had plugged all the micropores. The mean micropore diameter (less than 1 nm) and the relatively wide dispersion of their pore mouths within the mesopores [34], explains the small size and the strong retention of the Fe_2O_3 particles.

More generally, iron oxide particles were probably first deposited inside the micropores that exhibit the highest curvature for particle confinement, yielding a population of sub-nanometric isolated and well dispersed Fe_2O_3 particles when EDTA was used as iron oxide precursor. This effect was less marked for samples prepared using Fe(II)-gluconate and

(Fe(III),NH_4)-citrate complexes, in line with their less pronounced chelating efficiency. Finally, both the microporosity and the mesoporous volume of the parent SBA-15 was hardly affected by the more bulky Fe_2O_3 agglomerates stemming from the nitrate precursor.

The whole textural properties changes of the composites, as evaluated by TG-DTA in combination with other techniques, suggested that the chelating efficiency was in the following order: EDTA> citrate>gluconate>>nitrate, being understood that the more efficient the chelating power of the salt, the best their 'overcoating' the internal highly curved walls and the smaller the resulting Fe_2O_3 nanoparticles, because the Fe(III) cations remained very well dispersed and retained in the chelate precursors prior to their thermal degradation.

Nevertheless, thermal analysis alone could neither explain the small size nor the strong retention of the Fe_2O_3 particles generated by a strong chelate precursor such as (Fe(III),Na)-EDTA. Temperature-programmed reduction (TPR) experiments, used to evaluate the redox properties of Fe(III) species in the final composites, indicated that the ease of the Fe(III) reduction was another good probe to evaluate the retention strength of the initial Fe_2O_3 nanoparticles. Only one sharp reduction peak was observed for all the chelate- and nitrate-impregnated solids (Fig. 6). In each case, the quantitative evaluation of H_2 consumption revealed that the reduction of Fe(III) ended with the formation of Fe(II) (Table 4). This stabilization of FeO on the mesoporous silica is readily explained by considering that its basic character will favor its anchoring onto the acidic surface of the silica support, preventing either its preliminary stabilization as magnetite (Fe_3O_4) or its further reduction to metallic iron.

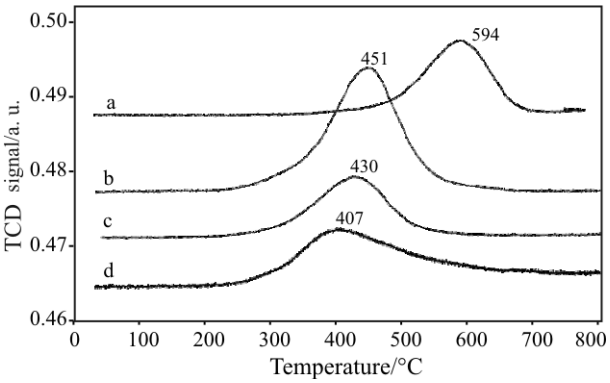

Fig. 6 H_2-TPR profile recorded for a – (Fe(III),Na)-EDTA/SBA-15, b – Fe(II)-gluconate/SBA-15, c – (Fe(III),NH_4)-citrate/SBA-15 and d – Fe(III)nitrate/SBA-15

The variation of the TPR temperature at which Fe(III) was reduced to Fe(II) (from 594°C for the composite prepared with Na-EDTA to 407°C for the sample prepared with iron nitrate) should be rather related to the interaction strength of the Fe_2O_3 particles with the support than to their size. In the case of the composite synthesized with iron nitrate, Fe_2O_3 particles of about 8 nm in diameter plugging the SBA-15 channels were reduced at a lower temperature than the far smaller particles generated after decomposition of the gluconate, citrate-NH_4 and especially Na-EDTA anions. Considering the sole particle size, one would have expected the reverse trend, namely that larger particles would have undergone reduction at a higher temperature than the nanometric sized ones. This apparent contradiction is easily explained here by considering that the Fe_2O_3 nanoslabs generated through the chelate decomposition are readily confined at the micropore mouths, because of their small size. The higher TPR temperature observed in the case of composites prepared using the chelate route is also in line with the chelating efficiency of the composites that is here directly related to several effects that characterize the final Fe_2O_3 particles: their (very small) size, their confinement at the micropore mouths that explains their strong retention on the support, as well as their regular dispersion on the silica internal surface.

While providing complementary information with respect to TPR, the electrochemical reduction of the same species determined by cyclic voltammetry similarly confirmed that the ease of Fe(III) reduction for all the chelate-impregnated solids was related to the retention strength of the initial Fe_2O_3 nanoparticles [27].

Catalytic behavior of silica-supported Fe_2O_3 nanoparticles generated by the chelate route

The TG-DTA results, along with the redox properties of the composites also suggest that the Fe_2O_3 nano-

Table 4 TPR characteristics (hydrogen consumption and iron reduction level) of various Fe_2O_3/SBA-15 composites

Sample (calcined)	Fe/mg g^{-1}	H_2 consumption/mL g^{-1}	Fe reduction level/%
(Fe(III),Na)-EDTA /SBA-15	35.9	6.93	32.2
Fe(II)-gluconate/SBA-15	39.6	7.51	31.6
(Fe(III),NH_4)-citrate /SBA-15	38.8	7.39	31.7
Fe(III) nitrate/SBA-15	38.1	7.81	34.0

particles obtained using the chelate route could be used as catalytic active centers for specific reactions, such as the total oxidation of phenol by H_2O_2 in aqueous medium and ambient conditions (Fenton reaction).

The catalytic reaction behavior obtained for the various Fe_2O_3/mesoporous silica composites is shown in Fig. 7 and Table 5. For all composites, the total phenol conversion was reached after 30 min of reaction and the TOC conversion level (total mineralization of the organic matter content) was similar (45%). Nevertheless a continuous leaching of iron species was observed in all cases. The low stability of these catalysts in aqueous medium is caused by the presence, in acidic solution, of intermediate reaction products (for example oxalic acid) leading to the complexation of Fe(III) ions, thus forming soluble moeities. The catalytic activity seems to be proportional to the iron species leaching rate. Except for the first phenol conversion step into the primary intermediate reaction products (i.e. hydroquinone, quinone) that proceeds in the heterogeneous phase, the presence of soluble iron species into the reaction medium accounts for a significant homogeneous catalytic contribution. This stems from an insufficient stabilization

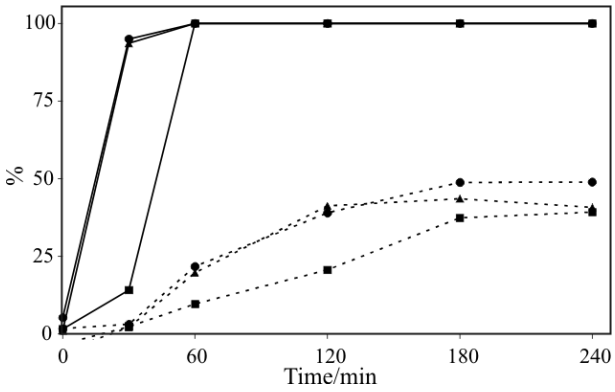

Fig. 7 Phenol oxidation by hydrogen peroxide over the Fe_2O_3/mesoporous silica synthesized following the chelate route at 25°C; — – phenol conversion; - - - – TOC abatement, ▲ – (Fe(III),Na)-EDTA/SBA-15, ■ – Fe(II)-gluconate/SBA-15 and ● – (Fe(III),NH_4)-citrate /SBA-15

of the Fe_2O_3 nanoparticles (weakly acidic oxide) inside the internal pore volume of the mesoporous silica (also weakly acidic oxide).

In order to prevent the metal leaching during the catalytic reaction, the interaction between the Fe(III) species and the substrate was further tested for other supports, such as mesoporous alumina or γ-Al_2O_3, that exhibits a more pronounced basic (amphoteric) character.

Fe_2O_3/mesoporous alumina composites prepared through the chelate route

Fe(III) chelates also interacted with the internal surface of an originally prepared [30] mesoporous alumina substrate (this work) and also within the textural porosity of γ-alumina [33].

In the typical example of (Fe(III),NH_4)-citrate impregnated on mesoporous alumina, combined TG-DTA again showed that the citrate anions decompose at lower temperatures (DTA main exotherm at 320°C) than when the iron citrate is free from any interaction (DTA exotherm at 370°C). As in the case of the same chelate adsorbed on mesoporous silica (DTA exotherm at 300°C), when the anions interact with the superficial Al–OH groups of the alumina surface, the citrate-Fe(III) bonds are more readily destabilized and Fe_2O_3 particles more promptly generated. As soon as these latter are freed from their chelating envelope, they will interact with the superficial Al–OH groups that show a more pronounced basic character than silanols. This stronger acid-base interaction between the two oxidic species would result in very small (XRD-silent and even TEM-silent) Fe(III)-based particles that could be depicted as either small stabilized $(Al,Fe)_2O_3$-type mixed species or possibly Fe(III) aluminate islets.

These mixed Al–Fe(III) oxides or Fe(III) aluminate domains proved very efficient catalytic centers for the aqueous phenol oxidation with hydrogen peroxide and extremely resistant to leaching (Table 5). While the Fe_2O_3/mesoporous silica composite synthesized with the (Fe(III),NH_4)-citrate che-

Table 5 Results of the catalytic wet peroxide oxidation of phenol over mesoporous Fe_2O_3/SBA-15 and Fe_2O_3/Al_2O_3 composites synthesized using the chelate route (T=25°C, unless otherwise specified)

Sample (calcined)	Phenol conversion after 4 h/%	TOC abatement after 4 h/%	Fe leaching after 4 h/mg L^{-1}
(Fe(III),Na)-EDTA/SBA-15	100	41	14.6
Fe(II)-gluconate/SBA-15	100	39	10.5
(Fe(III),NH_4)-citrate /SBA-15	100	49	14.1
(Fe(III),NH_4)-citrate/Al_2O_3 1st cycle	100	67	0.43
(Fe(III),NH_4)-citrate/Al_2O_3 2nd cycle	100	65	0.19
(Fe(III),NH_4)-citrate/Al_2O_3 (test performed at 40°C)	100	81	0.2

late was poorly efficient in terms of mineralization degree and stability (TOC conversion not exceeding 49% with a concentration of Fe leached of 14.1 mg L^{-1}), the corresponding Fe_2O_3/mesoporous alumina composite exhibited a TOC conversion of 67% with a very low leaching level of iron species (0.43 mg L^{-1}), which indicates that the active phase is stable in the reaction medium. With the purpose to quantify the effect of dissolved iron species in the reaction medium (homogeneous catalysis), the catalytic activity was evaluated in a solution containing 0.4 ppm of Fe^{3+}, giving rise to a minimum conversion (10%) after 4 h of reaction. Likewise, phenol conversion or TOC conversion were not observed in the absence of either catalyst or oxidant.

To prove the efficiency of the catalyst, a recycling study was also performed with the Fe_2O_3/mesoporous alumina composite prepared through the NH_4-citrate route. At the end of the first test, the catalyst was centrifuged and washed thoroughly several times, before being reintroduced inside the reactor without having been calcined. The catalytic reaction behavior (phenol conversion, TOC abatement and Fe leaching values) was shown to be totally similar during the second cycle of reaction, confirming the remarkable stability of the Fe_2O_3/mesoporous alumina composites (Table 5). The concentration of leached iron species was as low as 0.19 mg L^{-1} after the second cycle of reaction, confirming that the Fe(III)-based active sites were stabilized and strongly retained onto the mesoporous alumina surface due to a stronger acid-base interaction than with the mesoporous silica support.

When the reaction was performed at 40°C, the total organic carbon conversion (TOC abatement) was increased to 80%, still with very few soluble iron species (0.2 mg L^{-1}).

Such performances are required for efficient conversion of phenolic compounds in aqueous solution and for a reduced contamination of aqueous residues by transition metal ions stemming from leached catalysts.

Conclusions

Well dispersed (sub)nanometric Fe_2O_3 particles were generated inside the mesopores of SBA-15 silica and of mesoporous alumina substrates through their incipient wetness impregnation with less conventional iron precursors of the chelate type and the subsequent TG-DTA controlled calcination of the resulting composites.

The chelate complexes used in this study (EDTA, gluconate, citrate) proved particularly attractive to control the size and dispersion of the final Fe(III) oxidic particles. The bulkier the chelate, the smaller the resulting Fe_2O_3 particles.

Combined TG-DTA with N_2 adsorption-desorption measurements provided evidence that iron chelate precursors were stabilized through hydrogen-type interactions with the superficial silanols of the silica or with Al–OH end groups of the alumina substrate, during the drying step of the impregnated composites. This stabilization caused a decrease of the interaction of the chelate anions with their Fe(III) counterions, that were readily released and converted into (sub)nanometric Fe_2O_3 during calcination. Such particles were shown to preferentially interact with the highly curved internal walls of the mesoporous substrate (case of SBA-15 silica), more particularly near the micropore mouths, thereby leading to their eventual stabilization through a confinement effect.

When used as active sites in Fenton catalysis, such sub-nanometric Fe_2O_3 particles proved more particularly performant when supported on alumina than on silica because, as in the case of sub-nanometric Cu_2O deposited on mesoporous alumina [35], a better acid-base interaction could be achieved between the active phase and the support, thereby leading to the high dispersion and increased stabilization of such small particles.

References

1 G. Busca, L. Lietti, G. Ramis and F. Berti, Appl. Catal. B, 18 (1998) 1.
2 K. Sugawara, T. Nobukawa, M. Yoshida, Y. Sato, K. Okumura, K. Tomishige and K. Kunimori, Appl. Catal. B, 69 (2007) 154.
3 Y. Sun, S. Walspurger, J.-P. Tessonier, B. Louis and J. Sommer, Appl. Catal. A, 300 (2006) 1.
4 F. Arena, G. Gatti, G. Martra, S. Coluccia, L. Stivano, L. Spadaio, P. Famulari and A. Parmaliana, J. Catal., 231 (2005) 365.
5 D. H. Doff, N. H. Gangas, J. E. Allan and J. M. Coey, Clay Miner., 23 (1988) 367.
6 Y. Li, Z. Feng, H. Xin, F. Fan, J. Zhang, P. C. M. Magusin, E. J. M. Hensen, R. A. van Santen, Q. Yang and C. Li, J. Phys. Chem. B, 110 (2006) 26114.
7 E. Tronc, M. Nogues, C. Chaneac, F. Lucari, F. D'Orazio, J. M. Greneche, J. P. Jolivet, D. Fiorani and A. M. Testa, J. Magn. Magn. Mater., 272–276 (2004) 1474.
8 M. Luechinger, A. Kienhofer and G. D. Pirngruber, Chem. Mater., 18 (2006) 1330.
9 C.-Y. Liu, C.-F. Chen, J.-P. Leu and Y.-C. Lin, J. Sol-Gel Sci. Technol., 43 (2007) 47.
10 R. S. Prakasham, G. Sarala Devi, K. Raiya Laxmi and Ch. Subba Rao, J. Phys. Chem. C, 111 (2007) 3842.
11 A. Brăileanu, M. Răileanu, M. Crişan, D. Crişan, R. Bîrjega, V. E. Marinescu, J. Madarász and G. Pokol, J. Therm. Anal. Cal., 88 (2007) 163.

12 C. Messi, P. Carniti and A. Gervasini, J. Therm. Anal. Cal., 91 (2008) 93.
13 M. Ştefănescu, O. Ştefănescu, M. Stoia and C. Lazau, J. Therm. Anal. Cal., 88 (2007) 27.
14 B. Martinez, A. Roig, X. Obradors, E. Molins, A. Rouanet and C. Monty, J. Appl. Phys., 79 (1996) 2580.
15 S. Veintemillas-Verdaguer, M. P. Morales and C. J. Serna, Mater. Lett., 35 (1998) 227.
16 U. T. Lam, R. Mammucari, K. Suzuki and N. R. Foster, Ind. Eng. Chem. Res., 47 (2008) 599.
17 K. Bachari, J. M. M. Millet, P. Bonville, O. Cherifi and F. Figueras, J. Catal., 249 (2007) 52.
18 T. Abe, Y. Tachinaba, T. Uematsu and M. Iwamoto, Chem. Commun., (1995) 1617.
19 J. F. Bengoa, M. V. Cagnoli, N. G. Gallegos, A. M. Alvarez, L. V. Mogni, M. S. Moreno and S. G. Marchetti, Microporous Mesoporous Mater., 84 (2005) 153.
20 A. H. Jansen, C. M. Yang, Y. Wang, F. Schüth, A. J. Koster and K. P. de Jong, J. Phys. Chem. B, 107 (2003) 10552.
21 T. Tsoncheva, J. Rosenholm, M. Linden, F. Kleitz, M. Tiemann, L. Ivanova, M. Dimitrov, D. Paneva, I. Mitov and C. Minchev, Microporous Mesoporous Mater., 112 (2008) 327.
22 E. Delahaye, V. Escax, N. El Hassan, A. Davidson, R. Aquino, V. Dupuis, R. Perzynski and Y.L. Raikher, J. Phys. Chem. B, 110 (2006) 26011.
23 M. Fröba, R. Köhn, G. Bouffard, O. Richard and G. Van Tendeloo, Chem. Mater., 11 (1999) 2858.
24 G. R. Meima, B. G. Dekker, A. J. van Dillen, J. W. Geus, J. E. Bongaarts, F. R. van Buren, K. Delcour and J. M. Wigman, Stud. Surf. Sci. Catal., 31 (1987) 83.
25 D. J. Lensveld, J. G. Mesu, A. J. van Dillen and K. P. de Jong, Microporous Mesoporous Mater., 44–45 (2001) 401.
26 A. J. van Dillen, R. J. A. M. Terörde, D. J. Lensveld, J. W. Geus and K. P. de Jong, J. Catal., 216 (2003) 257 and references therein.
27 S. Valange, A. Charmot, J. Barrault, A. Louati and Z. Gabelica, Stud. Surf. Sci. Catal., 170A (2007) 531.
28 E. G. Derouane, J.-M. André and A. A. Lucas, J. Catal., 110 (1988) 58.
29 D. Zhao, J. Feng, Q. Huo, N. Melosh, G. H. Fredrickson, B. F. Chmelka and G. D. Stucky, Science, 279 (1998) 548.
30 S. Valange, J. L. Guth, F. Kolenda, S. Lacombe and Z. Gabelica, Microporous Mesoporous Mater., 35–36 (2000) 597.
31 J. Barrault, J. M. Tatibouet and N. Papayannakos, C. R. Acad. Sci. Paris, Série IIc, Chem., 3 (2000) 777.
32 S. Valange, Z. Gabelica, M. Abdellaoui, J. M. Classens and J. Barrault, Microporous Mesoporous Mater., 30 (1999) 177.
33 A. Charmot, Ph.D. Thesis, University of Poitiers, France 2006.
34 A. Galarneau, H. Cambon, F. Di Renzo, R. Ryoo, M. Choi and F. Fajula, New J. Chem., 27 (2003) 73.
35 S. Valange, A. Derouault, J. Barrault and Z. Gabelica, J. Mol. Catal. A, 228 (2005) 255.

DOI: 10.1007/s10973-008-9256-z